



1 Quantifying the impact of synoptic weather types and patterns 2 on energy fluxes of a marginal snowpack

3 Andrew Schwartz¹, Hamish McGowan¹, Alison Theobald², Nik Callow³

4 ¹Atmospheric Observations Research Group, University of Queensland, Brisbane, 4072, Australia

5 ²Department of Environment and Science, Queensland Government, Brisbane, 4072, Australia

6 ³School of Agriculture and Environment, University of Western Australia, Perth, 6009, Australia

7

8 Correspondence to: Andrew J. Schwartz (Andrew.Schwartz@uq.edu.au)

9

10 Abstract.

11 Synoptic weather patterns are investigated for their impact on energy fluxes driving melt of a marginal snowpack
12 in the Snowy Mountains, southeast Australia. K-means clustering applied to ECMWF ERA-Interim data identified
13 common synoptic types and patterns that were then associated with in-situ snowpack energy flux measurements.
14 The analysis showed that the largest contribution of energy to the snowpack occurred immediately prior to the
15 passage of cold fronts through increased sensible heat flux as a result of warm air advection (WAA) ahead of the
16 front. Shortwave radiation was found to be the dominant control on positive energy fluxes when individual
17 synoptic weather types were examined. As a result, cloud cover related to each synoptic type was shown to be
18 highly influential on the energy fluxes to the snowpack through its reduction of shortwave radiation and
19 reflection/emission of longwave fluxes. This research is an important step towards understanding changes in
20 surface energy flux as a result of shifts to the global atmospheric circulation as anthropogenic climate change
21 continues to impact marginal winter snowpacks.

22 1 Introduction

23 1.1 Synoptic weather influences on snowpack processes

24 Water generated in mountainous regions is a commodity that over 50% of the world's population depends on for
25 daily life (Beniston, 2003). Arguably, the most important role in the generation and regulation of these water
26 resources is that of montane snowpacks. These have been referred to as “water towers” (Viviroli et al., 2007) due
27 to their capabilities for storage and slow releases of meltwater. Many snowpacks are undergoing reductions in
28 spatial and temporal extent as a result of anthropogenic climate change (Pachauri et al., 2014). Understanding the
29 physical drivers of snowpack ablation, including synoptic-scale influences, is critical to help assess future water
30 resource availability in mountainous regions as climate change continues.

31 Snowfall has been related to synoptic weather types in numerous studies globally including in Athens (Prezerakos
32 and Angouridakis, 1984), the central and eastern United States (Goree and Younkin, 1966), the Tibetan Plateau
33 (Ueno, 2005), Budapest (Bednorz, 2008a), and the central European lowlands (Bednorz, 2011). However, work
34 on relationships between snowmelt and synoptic weather types is relatively scarce. Bednorz (2008b) identified
35 increased air temperature and rain-on-snow events as causes for rapid snowmelt ($> 5 \text{ cm day}^{-1}$) in the Polish-
36 German lowlands as a result of west-southwest airflows over Central Europe during positive phases of the North
37 Atlantic Oscillation (NAO). Similar work has been conducted in North America by Grundstein and Leathers
38 (1998) who were able to identify three main synoptic weather types responsible for significant snowmelt events
39 on the northern Great Plains, all of which included cyclonic influence with different low pressure centre locations
40 and warm air advection to the region. While some knowledge exists on synoptic drivers of snowpack ablation,



41 further research is needed to understand synoptic effects on ablation processes over snowpacks with varying
42 characteristics.

43 Marginal snowpacks are characterised by high snow density and internal temperatures, making them susceptible
44 to melt from energy input throughout much of the season and particularly sensitive to even subtle shifts in
45 available energy. Anthropogenic climate change has led to changes in snowpack and precipitation properties
46 globally (Adam et al., 2009; Stewart, 2009) and regions that have been historically categorized as having lower
47 temperatures have begun developing marginal characteristics as temperatures increase. However, research related
48 to synoptic influences on the surface energy balance over marginal snowpacks as defined by Bormann et al. (2013)
49 are rare. Hay and Fitzharris (1988) studied the influence of different synoptic weather types on glacier ablation
50 and snowpack melt, while Neale and Fitzharris (1997) used surface energy flux measurements to determine which
51 synoptic types resulted in highest ablation in the Southern Alps, New Zealand. These studies found net radiation
52 was the dominant term in ablation, but also noted that the contributions made by each term varied largely
53 depending on the synoptic type and its meteorology. A common characteristic between these studies and others
54 in various regions is that they focused primarily on the surface meteorology for synoptic classifications rather
55 than multiple level analysis, which enables insight to the potential influence of mid and upper-level atmospheric
56 conditions on surface – atmosphere energy exchanges. Regardless, no analysis at any level exists on synoptic type
57 influence on snowpack ablation within Australia.

58 **1.2 The Australian snowpack**

59 Characteristics of the snowpack in the Australian Alps have been examined in a number of studies with focus on
60 spatial and temporal snow cover variability (Budin, 1985; Duus, 1992), influence on catchment hydrology (Costin
61 and Gay, 1961), the energetics of snowpack melt (Bilish et al., 2018), and isotopic composition of precipitation
62 (Callow et al., 2014). Given observed declines in snow cover, climate change has become a central focus of this
63 research (Chubb et al., 2011; Hennessy et al., 2008; Nicholls, 2005; Reinfelds et al., 2014; Whetton et al., 1996) as
64 any changes to energy flux over the region will significantly impact the already marginal snowpack. Hennessy et
65 al. (2008) showed that future projections for the Australian snowpack predict reductions in annual areal snow
66 cover of 10-39% by 2020 and 22-85% by 2050. Observations indicate that reduction in snow cover is already
67 occurring with shortened annual periods of wintertime precipitation. Nicholls (2005) found reductions of 10%
68 and 40% in the maximum snow depth and snow depth at the first October measurement respectively from 1962
69 to 2002. In addition, wintertime precipitation was shown to have reduced by an average of 43% in high elevation
70 regions from 1990 to 2009 (Chubb et al., 2011), though much of this could have been due to several severe
71 droughts that occurred during the study period. Fiddes et al. (2015) showed that snowfall, snow accumulation,
72 and snow depth were highly correlated with temperature and that warming, as a result of climate change, could
73 lead to further reductions in the southeast Australia (SEA) snowpack. The importance of the water generated in
74 the Australian Alps, reduction in wintertime precipitation amounts and frequency, and high spatiotemporal
75 variability of snow accumulation and ablation (Budin, 1985) warrants an understanding of the energetics of
76 Australia's snowpack as they pertain to the influences of shifting synoptic-scale circulations.

77 **1.3 Synoptic weather types and trends in the Australian Alps**

78 The Australian Alps is a marginal snowpack environment (Bilish et al., 2019; Bilish et al., 2018), where
79 precipitation is crucial to agriculture, the generation of hydroelectric energy, and recreation and was estimated to



80 be worth \$9.6 billion per year in 2005 (Worboys and Good, 2011). A maximum in precipitation in the Australian
81 Alps typically occurs during the cooler months of June to September when it falls as snow at elevations above
82 1400 m, and accounts for twice as much precipitation as during the warmer periods of the year (Chubb et al.,
83 2011). While the snowpack typically exists for relatively short periods compared to those of other regions where
84 winter temperatures are lower and higher snowfall amounts occur such as parts of the European Alps and Rocky
85 Mountains, USA, it is still a vital resource for SEA.

86 Synoptic weather types in Australia have been changing in recent decades in response to the impact of climate
87 change on background climate states (Theobald et al., 2016;Hope et al., 2006). For example, increases in daily
88 maximum temperature and reductions in precipitation during autumn and winter have been noted in SEA as a
89 result of anomalously high surface pressure during positive periods of the Southern Annular Mode (SAM)
90 (Hendon et al., 2007). Cai et al. (2005) also showed an increase in SAM value as a response to all global warming
91 experiments using the CSIRO Mark 3 climate model indicating a further poleward shift in the location of synoptic
92 systems. However, it has been suggested that the SAM accounts for a relatively small portion of seasonal rainfall
93 variability in Australia and other larger impacts on synoptic weather from other sources are likely (Meneghini et
94 al., 2007).

95 Significant work has been conducted on identification of patterns and trends in Australian synoptic climatology
96 as it pertains to precipitation variability (Theobald et al., 2016;Chubb et al., 2011;Pook et al., 2014;2010;Pook et
97 al., 2006;2012). However, impacts on surface energy fluxes as a result of synoptic types have not been explored
98 as they have in other regions. The objective of this study is to identify the synoptic weather types that contribute
99 the highest amounts of energy to the Australian snowpack. This is accomplished through: 1) the identification and
100 classification of common synoptic types during periods of homogeneous snow cover, 2) attribution of snowpack
101 energy flux characteristics to each synoptic type, and 3) construction of energy balance patterns as they pertain to
102 common synoptic patterns/progressions.

103 2 Methods

104 2.1 Study site and climate

105 Energy flux measurements were made 16 km west of Lake Jindabyne at the Pipers Creek catchment headwaters
106 (36.417°S, 148.422°E) at an elevation of 1828 m in the Snowy Mountains, Kosciuszko National Park, New South
107 Wales (NSW), Australia (Figure 1). The catchment is classified as sub-alpine and contains grasslands, sub-alpine
108 bogs, and sub-alpine woodland (Gellie, 2005). The surrounding areas contain a mixture of living and dead
109 *Eucalyptus pauciflora* (Snow Gum) trees and open grassland areas with fens and alpine bogs. Many of the Snow
110 Gums were impacted by fire in 2003, and have experienced slow regrowth. The area's mixed characteristics of
111 forested and open grasslands with alpine wetlands within the Pipers Creek study catchment and immediately
112 surrounding the flux tower site used in this study are representative of those found throughout the Australian Alps.

113 The Snowy Mountains are characterized by relatively mild weather conditions compared to other mountain
114 ranges. Winter temperatures are typically around 0°C with mean low temperatures during July (the coldest month)
115 at -5°C and mean high temperatures between 2 to 4°C (Bureau of Meteorology, 2018b) that readily allow for melt
116 of the snowpack. As such, snowpack properties in the catchment are consistent with those of maritime snowpacks



117 that are associated with basal melting, high temperatures, and high wind speeds (Sturm et al., 1995; Bilish et al.,
118 2018).

119 The site chosen at the Pipers Creek catchment headwaters contains alpine bog and Eucalypt woodland that are
120 “the two most common types in the broader region, together representing 47% of the total area above 1400-m
121 elevation” (Bilish et al., 2018, p. 3839). Gellie (2005) showed that the *E. pauciflora* woodland was present in five
122 of the fifteen dominant vegetation formations that covers 57% of area within the broader region, while Alpine
123 grassland/bog (including herb fields) accounts for another 8%. Additionally, the study site was located at 1828 m
124 in the middle of the 1400-2228 m elevation range in the Australian Alps that typically has snowfall during the
125 winter allowing for measurements that apply broadly to other elevations. As with all single-site studies, there will
126 be some uncertainty when applying the energy balance to the wider area of the Australian Alps. However, this
127 should be reduced as the measurements made include surface types common in the wider region and were towards
128 the middle of the elevations that those conditions occur.

129 2.2 Instrumentation

130 The Pipers Creek site (Figure 2) was established on 10 June 2016 and collected data for the 2016 and 2017 winter
131 seasons. The site consisted of a Campbell Scientific eddy covariance (EC) system to measure fluxes of latent (Q_e)
132 and sensible (Q_h) heat at 10 Hz at a height of 3.0 m above ground level (AGL). A Kipp and Zonen CNR4
133 radiometer (3.0 m AGL) was used to measure incoming and outgoing shortwave (K) and longwave (L) radiation
134 to allow for comparisons of all radiation components rather than simply net all-wave radiation (Q^*). Ambient air
135 temperature and relative humidity were measured at the top of the mast by a Vaisala HMP155 probe at ~3.1 m
136 above ground level. A Hukseflux heat flux plate measured ground heat flux (Q_g) at a depth of 5 cm and was placed
137 approximately 0.5 m from the centre of the mast to minimize any influence the mast could have on snow
138 accumulation above the sensor. Surface temperatures were monitored using an Apogee Instruments SI-111
139 infrared radiometer at approximately 2 m from the centre of the mast. Details on the instruments used for each
140 measurement are shown in Table 1.

141 Precipitation data from an ETI Instrument Systems NOAH II weighing gauge located approximately 1 km to the
142 northwest of the energy balance site at elevation of 1761 m was supplied by Snowy Hydro Limited (SHL). A 6 m
143 diameter DFIR shield was used around the gauge in order to prevent wind-related under-catch of snowfall
144 (Rasmussen et al., 2012), and was additionally sheltered by vegetation to the west.

145 2.3 Identification of snow cover periods

146 Homogeneous snow cover is crucial to accurate measurement and analysis of snowpack energy balance (Reba et
147 al., 2009). Snow cover was considered to be homogeneous when no grass or bush was protruding from the snow
148 surface with the exception of distant patches of *E. pauciflora* trees. Periods with homogeneous snow cover were
149 determined using data from the Pipers Creek instrumentation site and were cross referenced to manual snow
150 measurements made at the Spencers Creek Snow Course 6.6 km northwest of the Pipers Creek field site (Snowy
151 Hydro Ltd, 2018). Periods with surface temperatures above 1.5°C as measured by the SI-111 infrared radiometer
152 that did not correspond to rain-on-snow events and periods with albedo measurements less than 0.40 (Robock,
153 1980) were considered to have heterogeneous snow cover and were eliminated.



154 **2.4 Synoptic classification of snow cover days**

155 Synoptic weather type classification of homogeneous snow cover days was conducted using synoptic typing
156 methods adapted from Theobald et al. (2015). European Centre for Medium-Range Weather Forecasts (ECMWF)
157 ERA-Interim reanalysis data (Dee et al., 2011) with a $0.75^\circ \times 0.75^\circ$ resolution was obtained for each day from 10
158 June 2016 through 31 October 2017. This date range was chosen to ensure inclusion of all potential dates with
159 snow cover during the 2016 and 2017 snow seasons after the initial instrument tower installation on 10 June 2016.
160 Variables included in the reanalysis data consisted of mean daily values of Mean Sea Level Pressure (MSLP);
161 temperature and relative humidity at 850, 700, 500, and 250 hPa; wind vectors at 10 m AGL, 850, 700, 500, and
162 250 hPa; and 1000-500 hPa geopotential heights. The domain of the included variables was limited to 20°S - 46°S
163 and 120°E - 160°E , ensuring coverage of synoptic scale systems affecting the Australian Alps.

164 Focus was placed on analysis of temperature (T_d) and relative humidity (RH) values because of their impact on
165 Q_e , Q_h , and radiative fluxes (Reba et al., 2009; Ruckstuhl et al., 2007; Allan et al., 1999; Webb et al., 1993). Relative
166 humidity values at 850, 700, and 500 hPa were used to investigate the potential influence of cloud cover. MSLP
167 and wind vector analysis at the 850, 700, 500, and 250 hPa levels allowed for the identification of T_d and RH
168 advection (Pook et al., 2006) into the Australian Alps. Thickness between 1000-500 hPa was used to determine
169 frontal positions relative to the Australian Alps (Pook et al., 2006) and accordingly the Pipers Creek field site.

170 The method used for synoptic comparison of energy flux characteristics was adopted from the approach of similar
171 types of studies (Theobald et al., 2016; Theobald et al., 2015; Chubb et al., 2011; Neale and Fitzharris, 1997) and
172 used “days” as the temporal period for analysis. “Days”, periods lasting twenty-four hours from 00Z to 23:59Z,
173 were considered optimal to determine radiative flux characteristics (diurnal radiation cycle) that may be missed
174 on smaller time scales. Similarly, the use of days allows for determination of short-term energy fluxes that can
175 also be easily compared over several months, thus being most appropriate for the entire snow season.

176 Days within the ERA-Interim data that matched snow cover days were extracted and analysed using the k-means
177 clustering algorithm developed by Theobald et al. (2015). The algorithm was tested for 1-20 clusters and an elbow
178 plot of the cluster distances was used to identify the optimum number of clusters (Theobald et al., 2015), which
179 was seven. The identification of an elbow in the plot at seven clusters indicates a reduction to the benefit of adding
180 additional clusters as the sum of distances for additional clusters fails to yield significant reductions beyond that
181 point (Wilks, 2011).

182 Clustering of the synoptic conditions for each day was verified through manual analysis of MSLP and 500 hPa
183 charts from the Australian Bureau of Meteorology (BOM) (Bureau of Meteorology, 2018). Cloud cover for each
184 type was investigated and verified through the use of visible band Himawari-8 satellite data
185 (<https://www.ncdc.noaa.gov/gibbs/>) at 03:00 UTC (13:00 local time) with one of three categories assigned to each
186 day studied; 1) no cloud cover, 2) partial cloud cover, or 3) complete cloud cover. Cloud cover was investigated
187 at midday to avoid misclassification due to short-lived clouds that appear over the area during the dawn and dusk
188 periods.

189 Manual verification of the k-means clustering algorithm using BOM synoptic charts identified four days (2.45%)
190 out of the 163 classified during the 2016 and 2017 seasons that had been classified incorrectly and they were
191 subsequently moved to their correct synoptic type. Three of the four misclassified days were early (7 June 2016)



192 or late (19 and 22 September 2016) in the snowpack seasons with the fourth occurring in the middle of winter on
193 31 July 2017. Synoptic characteristics from these days tended to be complicated with no discernible dominant
194 features that matched those of classified types. This is likely due to shifting synoptic conditions between seasons
195 related to poleward or equatorial shifts in westerly winds.

196 **2.5 Snowpack energy accounting**

197 Accurate measurement of snowpack energy balance and associated melt can be difficult due to snowpack
198 heterogeneity (Reba et al., 2009) and problems with energy balance closure (Helgason and Pomeroy, 2012). The
199 basic snowpack energy balance can be expressed as:

$$200 \quad Q_m = Q^* + Q_h + Q_e + Q_g + Q_r \quad (1)$$

201 where the energy available for snow melt (Q_m) is equal to the sum of Q^* , Q_h and Q_e , Q_g , and the energy flux to
202 the snowpack from liquid precipitation (Q_r) (Male and Granger, 1981; McKay and Thurtell, 1978). It's important
203 to note that all terms used in the calculation of the snowpack energy balance are net terms (Marks and Dozier,
204 1992; Stoy et al., 2018; Welch et al., 2016). Using net terms allows for conservation of energy within the (ideally)
205 closed energy balance system of the snowpack and aids in more accurately determining contributions of each term
206 to the energy balance.

207 Internal energy storage and melt processes can make calculation of the snowpack energy balance particularly
208 difficult when internal measurements of the snowpack are not available due to problems closing the energy
209 balance (Helgason and Pomeroy, 2012). This is particularly difficult over Australia's snowpack due to its marginal
210 characteristics that result in nearly constant internal snowpack melt. Therefore, Q_m can be more accurately
211 expressed as a residual energy term (Q_{res}) that is defined as the sum of the measured terms in Eq. (1) plus any
212 error in energy balance closure (Q_{ec}):

$$213 \quad Q_{res} = Q^* + Q_h + Q_e + Q_g + Q_r + Q_{ec} \quad (2)$$

214 While Q^* can be used for basic analysis of the snowpack energy balance, a decomposition into its individual
215 components is necessary to understand the role of short and longwave radiation exchange in snowpack energetics
216 (Bilish et al., 2018). Therefore, net radiation should be broken into its net flux terms:

$$217 \quad Q^* = K^* + L^* \quad (3)$$

218 that quantify the net shortwave (K^*) and net longwave (L^*) components.

219 The approach taken within this paper is to examine net radiative flux components individually, similar to the
220 methods used by Bilish et al. (2018), to be precise in the identification of synoptic-scale effects on snowpack
221 energy fluxes through differences in temperature, relative humidity, cloud cover. Q_{res} calculation and
222 comparisons of snowpack energy flux terms were performed using the terms in Eq. (2), but with the net radiation
223 terms (K^* and L^*) used rather than summed as Q^* only. This research uses the energy flux convention where
224 positive values are flux to the snowpack and negative values are flux away from the snowpack.



225 2.6 Energy flux measurements of synoptic types

226 Coordinate rotation for EC systems is typically used to account for errors introduced into flux data due to
227 imprecise instrumentation levelling. However, complex terrain can complicate EC measurements through local
228 scale processes such as thermally induced anabatic and katabatic flows, modification and generation of complex
229 terrain-induced flows, and inhomogeneity of terrain. In these areas, coordinate rotation is used to align the eddy
230 covariance coordinate system with the sloping surface and to identify and remove larger scale motions that may
231 be measured with the microscale flows. The Pipers Creek catchment site is located on predominantly level terrain,
232 however, double coordinate rotation was used to process the EC data to ensure terrain-induced influences on
233 airflow were removed (Stiperski and Rotach, 2016).

234 Frequency corrections were made to the EC data to account for sensor response delay, volume averaging, and the
235 separation distance of the sonic anemometer and gas analyser when calculating fluxes. Finally, WPL air density
236 corrections (Webb et al., 1980) were made to account for vertical velocities that exist as a result of changing air
237 mass density through fluxes of heat and water vapour. Quality flags were calculated for Q_h and Q_e using the
238 methods of Mauder and Foken (2011) that assigned a number from 0-2 based on the quality of the fluxes. High
239 quality data that is able to be used for fundamental research was assigned a 0, fluxes assigned a 1 are less accurate
240 but can still be used for long term observations, and fluxes assigned a 2 needed to be removed and gap-filled.

241 Q_h and Q_e flux were calculated using the EC equations:

$$242 \quad Q_h = -\rho C_p \overline{w'\theta'} \quad (4)$$

$$243 \quad Q_e = -\rho L_v \overline{w'q'} \quad (5)$$

244 where ρ is air density (kg m^{-3}), C_p is the specific heat of air ($1005 \text{ J kg}^{-1} \text{ deg}^{-1}$), $\overline{w'\theta'}$ is the average covariance
245 between the vertical wind velocity w (ms^{-1}) and potential temperature θ (K), L_v is the latent heat of sublimation
246 or vaporization of water (J kg^{-1}), and $\overline{w'q'}$ is the average covariance between the vertical wind velocity w (ms^{-1})
247 and specific humidity q (kg kg^{-1}) (Reba et al., 2009).

248 The calculation of Q_r followed Bilish et al. (2018) and was determined using three separate calculations to
249 establish approximate wet bulb temperature (T_w) (Stull, 2011), the fraction of precipitation falling as rain ($1 -$
250 P_{snow}) (Michelson, 2004), and total rain heat flux (Q_r) based on precipitation accumulation over a 30-minute
251 period.

252 2.7 Energy flux data quality control and gap-filling

253 In addition to removing EC measurements assigned a quality flag of 2, Q_e and Q_h values were also removed
254 when water vapour signal strength, a unit-less number calculated from the fraction of beam received compared to
255 that emitted, from the gas analyser was < 0.70 in order to remove erroneous readings during periods of
256 precipitation (Campbell Scientific, 2018; Gray et al., 2018). A seven point moving-median filter was implemented
257 over three iterations to de-spike the data and remove values more than 3.0 standard deviations away from the
258 median values.

259 Pre-existing gaps and gaps introduced into the data by the quality control procedures were filled using linear
260 interpolation described by (Falge et al., 2001a; 2001b) and the Random Forest regression technique (Breiman,



261 2001). Linear interpolation of missing Q_e and Q_h values was used for gaps up to 90 minutes in length.
262 Traditionally, mean diurnal variation values are also used for gap filling procedures (Falge et al.,
263 2001a;2001b;Bilish et al., 2018). However, it was determined that using mean values would likely obscure any
264 unique energy balance characteristics of the synoptic types being investigated and, therefore, was not included as
265 a gap-fill strategy for the data.

266 The R programming package randomForest (Liaw and Wiener, 2002) was used to fill gaps in Q_e and Q_h longer
267 than 90 minutes in length. The random forest regression trained to determine Q_e and Q_h flux values was developed
268 using twenty-six atmospheric and soil variables collected in addition to EC measurements. Mean squared errors
269 (MSE)'s were examined for forests with 1-500 trees and it was determined that 150 trees were sufficient to build
270 an accurate model for both Q_e and Q_h . Tests were then conducted to determine the optimal number of variables
271 to be randomly selected at each node that showed 13 variables was optimal for determination of Q_h and 14
272 variables should be used for Q_e . The Q_e and Q_h random forest regression models were tested for their ability to
273 predict values that had been used to train the models by comparing the measured Q_e and Q_h values with the
274 predicted values. Root Mean Squared Error (RMSE) and the Coefficient of Determination (R^2) were determined
275 for each advective flux. Predicted values showed high correlation to measured values with both variables showing
276 R^2 values higher than 0.97. The Q_e regression had a RMSE of 2.56 Wm^{-2} and had lower uncertainty than the Q_h
277 regression that had a RMSE of 4.67 Wm^{-2} .

278 Following quality control procedures, 2571 of the initial 7756 records (33%) remained in the Q_e data and 4019
279 records (52%) remained in the Q_h data. Linear interpolation yielded an addition of 910 Q_e values (12%) and 928
280 Q_h values (12%). The Random Forest regression models were the largest source of gap-filled data with the
281 contribution of an additional 4275 Q_e values (55%) and 2809 Q_h values (36%).

282 3 Results

283 Identification of homogeneous snow cover days for the 2016 and 2017 snow seasons (June to October) resulted
284 in 163 total days with 90 days occurring in the 2016 and 73 days in 2017. July, August, and September had the
285 highest number of classifiable days during the period. June and October still had periods with homogenous snow
286 cover, but they became intermittent and fewer classifiable days were in each of the months. This led to fewer
287 periods of study at the beginning and end of the snow seasons when the snowpack was variable, with more in the
288 late winter and early spring months when snow cover was more consistent. Mean surface and cloud characteristics
289 and median daily energy flux characteristics of synoptic types identified during the two seasons are presented in
290 Table 2.

291 3.1 Synoptic types

292 3.1.1 Surface characteristics

293 The dominance of the subtropical ridge in Australia's mid-latitudes is evident in the synoptic types. Four of the
294 types (T1,T2,T5 and T7) display dominant surface high pressure systems, each with slightly different orientation
295 and pressure centre locations (Figure 3a) resulting in different energy flux characteristics. Dominant south-
296 southwesterly winds from T1 are the result of the high pressure centre being located to the northwest of the study
297 area. T2 has a predominantly zonal flow resulting from an elongated high to the north-northeast. T5 and T7 are



298 characterized by north-northwesterly flow from high pressure centres over the New South Wales
299 (NSW)/Queensland (QLD) coast and directly over the Snowy Mountains region, respectively.

300 T3 is characterized as having dominant northwest winds along a trough axis that is positioned over SEA with a
301 secondary coastal trough extending from southern NSW to the NSW/QLD border. T4 shows a transition from a
302 surface trough that has moved to the east of the study region to a high pressure system that is moving into the area
303 with winds from both features that converge over the Snowy Mountains region. The only synoptic type to have
304 dominant influence from a surface low was T6 that had weak south-southwesterly flow over the region from a
305 weak cut-off low to the east. For the purposes of this research, the identification of cut-off lows follows the
306 characteristics outlined by Chubb et al. (2011) that omits the presence of a closed circulation, but includes a cold
307 anomaly aloft that was cut off from the westerly wind belt.

308 Though characterization of synoptic types is purely statistical, T1, T4, T5, and T6 are considered to be ‘transition
309 types’ as they have surface pressure characteristics that indicate a change in pressure regime (low – high or high
310 – low) in the upcoming days. T1, T4, and T6 are post-frontal transition types that show high pressure ridging into
311 the region following the passage of a trough that has either moved to the east (T1 and T4) or developed into a
312 weak lee-side cut-off low (T6). T5 shows the approach of a trough from the west and an associated transition to
313 a low pressure system. T2 and T7 show the area under the influence of zonal flow as a result of high pressure
314 systems centred over the area, while T3 shows SEA under the influence of a trough at the time of observations.

315 **3.1.2 Relative humidity and cloud cover**

316 Understanding RH values associated with different synoptic types provides the ability to track types that are
317 favourable for high Q_e exchange with the snowpack. In addition, RH values at all tropospheric levels can have
318 impacts on snowpack energy flux through influences on K^* and L^* exchange via changes to insolation and the
319 absorption and emission of L . The identification of RH characteristics and associated cloud cover is necessary to
320 fully develop energy flux characteristics for each type.

321 Many of the synoptic types display local RH maxima in the Snowy Mountains region at 850 hPa (Figure 3b) and,
322 while T5 has the lowest RH values of all types, it still has slightly higher RH values over the area. The elevation
323 in RH values in the region is most likely caused by changes of airmass thermodynamic properties due to
324 orographic forcing of the mountains (Ahrens, 2012). T4 and T6 had the highest RH values over the region at 850
325 hPa with both being widespread and higher than 90%. T6 shows strong southerly advection of elevated RH values
326 from the tropics along the NSW and QLD coast ahead of troughs at 700 and 500 hPa that are associated with the
327 surface cut-off low.

328 Identification of cloud cover, conducted following the procedures outlined in section 2.4, agreed with the mean
329 RH characteristics of T4 and T6 with both types having 100% cloud cover between partial and complete cloud
330 cover days (Table 2). T6 showed the highest RH values of any type with values greater than 90% over the region
331 at the 700 and 500 hPa levels. While not definitive, this would suggest that T6 has deeper or more cloud layers
332 than T4, which likely only has clouds at lower altitudes. T2 and T7 had the lowest percentage of days with any
333 cloud cover, which is confirmed by their low RH values at 700 hPa (<20% & <30%) and 500 hPa (<30% &
334 <40%), respectively. In addition, they also had the highest percentage of cloud-free days with T2 clear sky 19%



335 of the time and T7 having 23% of its days without cloud. The remaining types (T1, T3, and T5) showed a relatively
336 consistent number of cloud days based on the satellite observations that were all above 85%.

337 **3.1.3 Temperature**

338 Temperature characteristics of synoptic types at low and mid-levels in the atmosphere are crucial to identify those
339 with the highest surface sensible heat flux characteristics. The highest mean temperatures and strongest warm air
340 advection (WAA) in the Snowy Mountains region at 850 hPa (Figure 3c) was found to be from T5 that is driven
341 by converging winds on the back of a high pressure circulation to the east and the leading edge of a trough to the
342 west. T2 and T3 have the second and third highest temperatures, respectively, but have different advection
343 characteristics. T2 shows relatively weak WAA into the Snowy Mountains region associated with zonal flows at
344 850 hPa resulting from the high pressure circulations located to the north (similar to T7). However, T3 shows cold
345 air advection (CAA) associated with dominant winds from the west-northwest.

346 Overall, CAA at 850 hPa can be identified in four of the seven types (T1, T3, T4, and T6) and warm air advection
347 exists in the other three synoptic types (T2, T5, and T7). Of the four CAA types, T1 and T4 advection is being
348 generated through south-southwest and west-southwest winds, respectively, related to high pressure centres to the
349 northwest. Despite a stronger southerly component of dominant CAA winds in T1, temperatures are lower in T4
350 which has a higher westerly component to the wind. T6 shows CAA related to converging winds on the back of a
351 trough to the east and a high to the northwest.

352 **3.1.4 Frequency and duration**

353 The frequency of each synoptic type during the 2016 and 2017 snowpack seasons is shown in Table 2. T3 and T7
354 occurred most frequently with 26.99% (44 days) and 19.02% (31 days) respectively. The higher number of days
355 in T3 and T7 is reflected in the mean type duration that shows these types with the longest duration. This is likely
356 due to these synoptic types occurring in a slower progressing synoptic pattern over multiple days as seen in the
357 mean type duration data (Table 2).

358 Transition probabilities for the 2016 and 2017 seasons were developed similar to those used by Kidson (2000)
359 that detail the likelihood of a synoptic type occurring on the following day given an initial type. The highest
360 transition probabilities were identified for each type and a flowchart was developed based on the most likely
361 synoptic type progressions (Figure 4a). If the highest transition probabilities were within < 0.05 of each other, two
362 paths were plotted. The flowchart shows what would be expected for a basic synoptic-scale circulation at mid-
363 latitudes; a trough propagating eastward into the Snowy Mountains region in T7, T5, and T3; either continued
364 eastward movement of the surface trough (T4) or the development of a weak cut-off low (T6); then transitioning
365 to dominant high pressure over the region again (T2, T1, or T7).

366 **3.2 Energy flux characteristics of synoptic types**

367 It is important to consider the effects of synoptic type frequency when determining primary sources of energy
368 fluxes over long periods, as synoptic types that contribute the most to snowpack ablation may simply have a higher
369 rate of occurrence and lower daily energy flux values than other types. In order to obtain a more detailed
370 understanding of each type's energy flux, median daily energy flux calculated for each type was determined to be
371 a better method of comparison. Therefore, both median daily and total snowpack fluxes over the two seasons
372 (Figures 5 & 6) are presented in MJ m^{-2} to show synoptic type energy flux contributions made at short and longer



373 temporal scales. While initial measurements were made in Wm^{-2} , the use of MJ m^{-2} in this paper allows for easier
374 comparison to other energy balance works conducted on this region (Bilish et al., 2018) as well as research on
375 synoptic weather and energy fluxes in other locations (Welch et al., 2016; Burles and Boon, 2011; Ellis et al.,
376 2011; Hay and Fitzharris, 1988; McGregor and Gellatly, 1996; Granger and Gray, 1990; Neale and Fitzharris, 1997).

377 3.2.1 Latent and sensible heat flux

378 Daily Q_e was negative for each of the seven synoptic types (Figure 5a) and the magnitude of the values was shown
379 to correspond to the mean 850 hPa RH values for each type reflecting the site elevation of 1828 m asl. Two of the
380 three types with the lowest RH values (T2 and T5) showed the greatest negative Q_e values and those with the
381 higher RH values (T1 and T6) showed the least amount of Q_e , which is consistent with conditions needed for
382 evaporation from the snowpack. T5 had the second largest negative Q_e values of any type with a median value
383 of $-1.00 \text{ MJ m}^{-2} \text{ day}^{-1}$ which corresponds to its low 850 hPa RH values, the highest observed surface mean daily
384 ambient temperature of $3.5 \text{ }^\circ\text{C}$, and the second lowest observed surface mean RH value of 65% with only T2 being
385 lower (60%). T3 showed the largest release of Q_e from the snowpack with a median value of $-1.11 \text{ MJ m}^{-2} \text{ day}^{-1}$.

386 Overall, negative Q_e was offset by positive Q_h for most synoptic types with the exception of T3 that had mean
387 surface temperatures below zero (-0.83°C) and a measured surface RH value below 90% resulting in more Q_e
388 loss than Q_h gain by the snowpack. Similar to trends seen in Q_e , the highest daily median Q_h values (Figure 5b)
389 were associated with synoptic types with the highest temperatures at 850 hPa (T5, T7, & T2), which coincided
390 with observed temperatures from the energy flux tower (3.48°C , 1.46°C , & 1.89°C). T5 showed the highest daily
391 Q_h values as a result of having the highest temperatures and also has the second lowest Q_e value that is associated
392 with having the lowest RH of any type (60%). Ultimately, when both turbulent terms are considered, T5 had the
393 highest amount of energy flux into the snowpack ($1.49 \text{ MJ m}^{-2} \text{ day}^{-1}$) followed by T7 ($1.40 \text{ MJ m}^{-2} \text{ day}^{-1}$) and T1
394 ($1.00 \text{ MJ m}^{-2} \text{ day}^{-1}$).

395 3.2.2 Radiation flux

396 The largest contribution of radiative energy to the snowpack from all synoptic types was K^* which accounted for
397 53-97% of total positive flux (Figure 5c). By comparison, L^* accounted for 61-95% of negative energy flux from
398 the snowpack (Figure 5d) with the highest amounts of loss belonging to the types with the lowest percentage of
399 cloud cover (T1, T2, and T7). Total radiation flux varied largely by synoptic type and was found to be positive in
400 types T3 and T6 and negative for the rest of the types. The two types with positive net radiation had the highest
401 incoming longwave radiation flux values mostly balancing outgoing longwave values. This meant that incoming
402 shortwave radiation to dominates Q^* . The largest loss in Q was exhibited by T1, that was 31% higher than the
403 next closest type (T4). The types with net radiation loss (T1, T2, T4, T5, and T7) had values that ranged from -
404 $0.67 \text{ MJ m}^{-2} \text{ day}^{-1}$ (T5) to $-2.78 \text{ MJ m}^{-2} \text{ day}^{-1}$ (T1). However, T4 had dissimilar cloud and RH characteristics to
405 T2 and T7, which had the two lowest cloud cover percentages and two of the lowest RH values. T4 had 100%
406 cloud cover and had an associated reduction in incoming shortwave radiation that allowed the outgoing longwave
407 radiation term to become more dominant than in T2 or T7 and, therefore, gave it the highest Q^* loss of the three.

408 3.2.3 Ground and precipitation heat flux

409 Energy flux from ground and Q_r (Figure 5e & 5f) were the smallest of any term for all synoptic types, with Q_g
410 and Q_r accounting for less than one percent of median daily energy fluxes for all synoptic types. Ground heat flux



411 characteristics were similar between all synoptic types and varied little. While Q_r was small when examined as a
412 daily median value, it does show a high degree of variation primarily associated with T5 and T3. This is due to
413 several large rain events that occurred during 2016 (18 July; 21 and 22 July; and 31 August) and one during 2017
414 (15 August). Despite relatively low energy flux contributions by rainfall, it is interesting to note that the ten days
415 with the highest rainfall fluxes ($>0.05 \text{ MJ m}^{-2} \text{ day}^{-1}$) consisted of four T5 days, three T3 days, two T7 days, and
416 one T6 day showing a significant clustering of high precipitation days in types T5 and T3.

417 3.2.4 Total daily net energy flux

418 Overall, two synoptic types (T5 and T6) had positive median daily net energy flux to the snowpack (Figure 6a).
419 Of these, T5 had the largest energy flux that was related to its relatively high temperatures that contributed to the
420 highest Q_h value of any synoptic type and increased solar radiation from less cloud cover. Contrary to the reduction
421 in cloud cover that aided T5 in having the highest total energy flux contributions, T6 had the highest cloud cover
422 and yet had the second highest energy flux to the snowpack that was primarily due to increased incoming
423 longwave radiation. T7 was close to having neutral energy fluxes with a median value of only $-0.04 \text{ MJ m}^{-2} \text{ day}^{-1}$
424 as a result of relatively low percentage of cloud cover resulting in strongly negative L^* as well as the second
425 highest Q_h term of any type.

426 T1 and T4 showed the greatest negative median daily net energy flux of all synoptic types (Figure 6a), which
427 could be attributed to their negative L^* and to having low K^* terms. T3 has a similar net energy flux to T4, but is
428 negative primarily due to having the only negative Q_h of any type. T2 also had a net negative median daily energy
429 flux but to a lesser extent than either T1, T3, or T4. Relative humidity values lower than any other type were the
430 primary driver behind T2's negative net value as it resulted in the highest longwave radiation loss from the
431 snowpack through having the lowest cloud cover, as well as Q_e loss.

432 The synoptic type T5 contributed the most energy to the snowpack during the two seasons (Figure 6b) due to a
433 high number of occurrences (24) and having the largest positive fluxes from high Q_h values associated with strong
434 WAA ahead of the passage of cold fronts. While T6 was the only other type to have positive median daily energy
435 flux contributions to snowpack energy flux, T7 contributed a higher amount of energy flux during the two winter
436 periods because it had the second highest number of occurrences, and the distribution of occurrences around the
437 median show that events were either near-neutral or positive in their energy fluxes. T6 was the only other type to
438 have a positive energy flux contribution to the snowpack over the two seasons and it was smaller than that of T5
439 or T7. Similar magnitude was seen in the negative flux contributions of T1, T2, and T4 with T2 having the most
440 significant negative flux. T1 and T4 also showed negative fluxes, but T3 showed a nearly neutral contribution to
441 snowpack energy flux over the two winter seasons. As T3 is associated with a surface trough, it's possible that
442 pre-frontal and post-frontal characteristics are both incorporated in the energy balance of T3 and act to cancel
443 each other out when averaged over a longer period.

444 All synoptic types had variation in median daily net energy that can be attributed to the classification conducted
445 by the k-means clustering technique. Each type consisted of classified days that had similar synoptic
446 characteristics, but differences in system strength and position affected energy fluxes for individual days.
447 Therefore, it is important to remember that each synoptic type is associated with a range of daily energy flux
448 values in addition to the median daily energy flux for each type.



449 **4 Discussion**

450 **4.1 Properties of synoptic type energy balance**

451 Net shortwave radiation flux contributed the largest amount of energy to the snowpack for all synoptic types
452 ranging from 53-97% of median daily energy flux with T5 being the only synoptic type below 60% contribution
453 (53%) of K^* to the snowpack. These results agree with Fayad et al. (2017) who noted that radiative fluxes are the
454 dominant source of snowpack melt energy in mountain ranges with Mediterranean climates. Net Q_h contributed
455 the second highest percentage of median daily energy flux to the snowpack accounting for 16-44% of positive
456 fluxes with the exception of T3 that had a Q_h term that accounted for 4% of its negative fluxes. The largest
457 contributions of Q_h to the snowpack are associated with synoptic types T2, T4, T5, and T7 that are characterised
458 by high pressure and northwesterly or westerly winds that are associated with WAA. Hay and Fitzharris (1988)
459 noted that, while radiative terms were responsible for the majority of energy contributions to glacier melt in New
460 Zealand's Southern Alps, turbulent fluxes contributed significant amounts of energy to melt. Similarly, despite
461 Q_h not being the dominant energy flux to the snowpack for any synoptic type, it does account for nearly half of
462 the energy flux to the snowpack for T5 (44%) and over a third for T7 (35%), and is still a significant source of
463 energy flux to the snowpack for nearly all synoptic types.

464 Median daily energy loss from the snowpack was from Q_e and Q^* , which dominated T1, T2, and T4 resulting in
465 negative median daily energy fluxes from the snowpack. Net longwave radiation was the most influential term in
466 the emission of energy from the snowpack accounting for 61-95% of energy loss with net Q_e flux accounting for
467 5-39% of outgoing energy flux. Though the methodology of this paper distinguishes between shortwave and
468 longwave fluxes in order to better examine the effects of synoptic-scale features such as RH or cloud cover on
469 radiative transfers similar to that of more recent works such as Cullen and Conway (2015), many historical works
470 have not made the same distinction in terms (Moore and Owens, 1984; Hay and Fitzharris, 1988; Neale and
471 Fitzharris, 1997; Stoy et al., 2018). It should be noted that had Q^* been used for comparison, the results of this
472 paper agree with several studies (Sade et al., 2014; Moore and Owens, 1984; Bednorz, 2008b) that found that
473 turbulent fluxes were the dominant fluxes when examining the energy flux characteristics on snowpacks in
474 climates similar to that of the Snowy Mountains in the Australia Alps.

475 Median daily Q_g values were found to account for only a small fraction of total energy flux to the snowpack
476 consisting of 1-5% of daily positive energy fluxes. Similarly, energy flux to the snowpack from Q_r has been
477 shown to only contribute < 1% of total seasonal energy flux for five of the seven synoptic types which agrees with
478 the findings of other studies (Bilish et al., 2018; Mazurkiewicz et al., 2008). However, precipitation was
479 responsible for > 1% of the daily median energy flux of the two synoptic types primarily associated with rain-on-
480 snow events, T5 and T3. Although fluxes imparted on the snowpack from rainfall are relatively small when
481 compared to all positive fluxes, the accompanying energy flux characteristics of T5 associated with rain-on-snow
482 events are responsible for two of the three largest contributions of overall snowpack energy fluxes.

483 The results show a significant agreement with previous research conducted in this region by Bilish et al. (2018)
484 when methods from that work are used to calculate relative contributions of positive energy fluxes to the
485 snowpack. Overall, incoming longwave radiation was shown to be the highest positive flux to the snowpack
486 accounting for 75-86% of incoming energy flux. Shortwave radiation was responsible for an additional 8-14% of



487 incoming energy flux with Q_h accounting for 0-9% of incoming fluxes, Q_e generating 0-4%, Q_g attributing 0.3%,
488 and Q_r accounting for 0.1%. Despite methodological differences that can be attributed to the need to highlight
489 different processes within atmosphere – snowpack interaction, results from both papers show similar overall
490 energy fluxes.

491 **4.2 Synoptic patterns and energy flux**

492 Snowpack energy flux characteristics recorded at the Pipers Creek catchment headwaters have been related to
493 synoptic weather types that occurred during the 2016 and 2017 snow seasons. The resulting analysis reveals a
494 maximum in positive energy flux as pre-frontal troughs approach the Snowy Mountains, followed by cold front
495 conditions during the T7→T5→T3 common progression pattern identified here. Several factors cause high
496 positive energy flux during these periods that include: an increase in temperatures due to WAA and the associated
497 increase in positive Q_h ; decrease in negative L^* due to an increase in cloud cover; a decrease in Q_e following
498 frontal passage and associated increase in RH; and progressively increasing Q_r as the trough approaches and
499 immediately after passage.

500 Synoptic types characterized by surface high pressure as their primary influence (T1, T2, T4, and T7) had four of
501 the five negative daily contributions to snowpack energy flux. In T1, T2, and T7, net shortwave radiation terms
502 (K^*) were positive and varied by ~4-10% for these types, however, low RH and cloud cover allowed for highly
503 negative L^* terms that were not compensated by change in K^* . In contrast, T4 had higher cloud cover and increased
504 RH that were due to advection of moisture from the Tasman Sea. The higher RH in T4 and low mean air
505 temperature (-2.06°C) resulted in Q_e and Q_h terms of similar magnitudes, but opposite signs that nearly cancelled
506 out. This resulted in a L^* term that was of lesser magnitude than those of T1, T2, and T7, but still the dominant
507 term in its energy exchange.

508 Four primary synoptic circulation patterns were identified during the study period. Each of the four patterns and
509 their associated energy flux values calculated from median daily flux and mean type duration can be seen in
510 Figures 4a and 4b. While each pattern differs towards the end of the cycle, each one has the T7→T5→T3
511 progression in common. Unsurprisingly, the highest contribution of median energy flux to the snowpack (0.75 MJ
512 m⁻²) is from Pattern 1, which has only one synoptic type with negative flux (T3) whereas the others all contain
513 multiple negative flux types. Pattern 3 had the largest negative snowpack energy flux (-2.44 MJ m⁻²) due to it
514 containing types with the highest net energy loss (T1 and T4).

515 Changing synoptic regimes in the Snowy Mountains suggest an increase in anti-cyclonic conditions (Hendon et
516 al., 2007), such as types T1, T2, T4, and T7, as a result of poleward shift in the subtropical ridge (Cai et al., 2005).
517 Under these conditions, snowpack energy exchange in the Australian Alps would be expected to decrease as
518 synoptic types related to anti-cyclonic conditions have negative energy fluxes to the snowpack and synoptic
519 patterns T3 and T4, which have the largest negative snowpack energy fluxes, would increase in frequency. While
520 these results may seem counterintuitive regarding a generally warming climate, they agree with the findings of
521 Theobald et al. (2016) who showed reductions in cool-season precipitation amounts and frequency due, in part,
522 to reductions in the occurrence of dominant cold front systems. The reduction in cold-frontal systems in the
523 Australian Alps region is associated with declines in the pre-frontal WAA that has been shown to be the primary
524 driver of positive snowpack energy flux. However, potential reductions in energy fluxes to the snowpack will not



525 likely lead to increases in snowpack duration or depth, as reductions in precipitation are associated with the shifts
526 to anti-cyclonic synoptic patterns (Theobald et al., 2016;Theobald et al., 2015).

527 **4.3 Distribution of gap-filled eddy covariance fluxes**

528 One of the disadvantages of the Random Forest regression method to gap-fill missing EC data is that exact results
529 aren't reproducible due to the method's random handling and sub-setting of predictor variables. Methods of
530 developing models and predicting values were evaluated over twenty iterations to determine the amount of
531 variability in RMSE when generating a random forest from the same dataset. Some variability in RMSE was noted
532 between tests for Q_e and Q_h but was small with a standard deviation of 0.01 Wm^{-2} in Q_e and 0.03 Wm^{-2} in Q_h .
533 Small differences in RMSEs between model development runs and data filling indicate that RMSE values for gap-
534 filled data would be best represented as $2.56 \pm 0.01 \text{ Wm}^{-2}$ for Q_e and $4.67 \pm 0.03 \text{ Wm}^{-2}$ for Q_h

535 Gap-filling of Q_h and Q_e can introduce uncertainty into measurements that may affect the ability to thoroughly
536 compare datasets such as those pertaining to the different synoptic types compared within this work. As such, it
537 is important to note that not all synoptic types had equal amounts of gap-filling for their Q_e and Q_h fluxes.
538 Distribution of gap-filled data within synoptic types depended largely on the quantity of precipitation associated
539 with each type. The most significant concentrations of gap-filled data were in T3 (Q_e : 74%, Q_h : 55%) T5 (Q_e :
540 57%, Q_h : 39%), and T6 (Q_e : 81%, Q_h : 73%). Differences in the quantity of gap-filled data between synoptic types
541 can create uncertainty when making comparisons between fluxes in each. However, uncertainty introduced
542 through gap-filling procedures is relatively low and should have a minimal impact during comparison of fluxes.

543 **5 Conclusions**

544 Overall, periods of pre-cold frontal passage contribute the most energy fluxes to snowpack melt due to WAA
545 ahead of the front, a reduction in cloud cover allowing for higher incoming shortwave radiation, and the gradual
546 development of precipitation that often contributes to rain-on-snow events. While this work was conducted solely
547 on the Australian snowpack, snowpacks in other regions such as New Zealand (Hay and Fitzharris, 1988;Neale
548 and Fitzharris, 1997), Canada (Romolo et al., 2006a;2006b), the Spanish Pyrenees (Lopez-Moreno and Vicente-
549 Serrano, 2007), and the Arctic (Drobot and Anderson, 2001) see similar synoptic-scale effects on snowpack
550 energy to those presented here. Snowpack energy fluxes in the Australian Alps would likely decrease under
551 climate change progression as a result of reductions to primary cold-frontal systems and associated pre-frontal
552 WAA.

553 The understanding of synoptic-scale processes on snowpack energy balances will likely become applicable to
554 broader regions as climate change continues and snowpacks develop warmer properties (Stewart, 2009;Adam et
555 al., 2009). An increased burden on freshwater systems for agriculture, drinking water, and energy production will
556 continue as these changes occur (Parry et al., 2007). Therefore, continued work on marginal snowpack ablation
557 processes, such as those within the forested regions of Australia's Snowy Mountains, will be important to resource
558 management and should be explored.

559 **Data Availability**

560 Energy flux data used in this study is available at <https://doi.org/10.14264/uql.2019.691>. ERA-Interim reanalysis
561 data are freely available from the European Centre for Medium-Range Weather Forecasts
562 (<https://www.ecmwf.int/en/forecasts/datasets/reanalysis-datasets/era-interim>). Precipitation data used in this



563 study was supplied by Snowy Hydro Limited via restricted access, this data can be obtained by contacting Snowy
564 Hydro Ltd.

565 **Author Contributions**

566 AS, HM, AT, and NC designed the experiments and AS conducted them. AT developed the k-means clustering
567 and synoptic typing code. AS developed the code related to energy balance and eddy covariance measurements.
568 AS wrote the manuscript with input from all authors.

569 **Competing Interests**

570 The authors declare that they have no competing interests.

571 **Acknowledgements**

572 The authors would like to thank Shane Bilish for establishment of the Pipers Creek snowpack research catchment,
573 Michael Gray for installation and maintenance of the energy balance tower, and the Weather and Water team at
574 Snowy Hydro Limited for their contributions of data and field support during the data collection and analysis
575 process. AS was supported by an Australian Government Research Training Program Scholarship.

576

577

578

579



580 **References**

- 581 Adam, J. C., Hamlet, A. F., and Lettenmaier, D. P.: Implications of global climate change for snowmelt hydrology
582 in the twenty-first century, *Hydrological Processes: An International Journal*, 23, 962-972, 2009.
- 583 Ahrens, C. D.: *Meteorology today: an introduction to weather, climate, and the environment*, Cengage Learning,
584 2012.
- 585 Allan, R. P., Shine, K. P., Slingo, A., and Pamment, J.: The dependence of clear-sky outgoing long-wave radiation
586 on surface temperature and relative humidity, *Quarterly Journal of the Royal Meteorological Society* 125, 2103-
587 2126, 1999.
- 588 Bednorz, E.: Synoptic conditions of snow occurrence in Budapest, *Meteorologische Zeitschrift*, 17, 39-45,
589 10.1127/0941-2948/2008/0262, 2008a.
- 590 Bednorz, E.: Synoptic reasons for heavy snowfalls in the Polish–German lowlands, 92, 133-140, 2008b.
- 591 Bednorz, E.: Synoptic conditions of the occurrence of snow cover in central European lowlands, 31, 1108-1118,
592 2011.
- 593 Beniston, M.: Climatic Change in Mountain Regions: A Review of Possible Impacts, *Climatic Change*, 59, 5-31,
594 10.1023/a:1024458411589, 2003.
- 595 Bilish, S. P., McGowan, H. A., and Callow, J. N.: Energy balance and snowmelt drivers of a marginal subalpine
596 snowpack, *Hydrol Process*, 32, 3837-3851, 2018.
- 597 Bilish, S. P., Callow, J. N., McGrath, G. S., and McGowan, H. A.: Spatial controls on the distribution and
598 dynamics of a marginal snowpack in the Australian Alps, *Hydrol Process*, 33, 1739-1755, 10.1002/hyp.13435,
599 2019.
- 600 Bormann, K. J., Westra, S., Evans, J. P., and McCabe, M. F.: Spatial and temporal variability in seasonal snow
601 density, *J Hydrol*, 484, 63-73, 2013.
- 602 Breiman, L.: *Random Forests*, *Machine Learning*, 45, 5-32, 10.1023/a:1010933404324, 2001.
- 603 Budin, G.: Interannual variability of Australian snowfall, *Aust. Met. Mag.*, 33, 145-159, 1985.
- 604 BOM: Analysis Chart Archive: <http://www.bom.gov.au/australia/charts/archive/>, access: 15.09.2018, 2018.
- 605 Burles, K., and Boon, S.: Snowmelt energy balance in a burned forest plot, Crowsnest Pass, Alberta, Canada,
606 *Hydrol Process*, 25, 3012-3029, 10.1002/hyp.8067, 2011.
- 607 Cai, W., Shi, G., Cowan, T., Bi, D., and Ribbe, J.: The response of the Southern Annular Mode, the East Australian
608 Current, and the southern mid-latitude ocean circulation to global warming, 32, doi:10.1029/2005GL024701,
609 2005.



- 610 Callow, N., McGowan, H., Warren, L., and Speirs, J.: Drivers of precipitation stable oxygen isotope variability in
611 an alpine setting, Snowy Mountains, Australia, *Journal of Geophysical Research: Atmospheres*, 119, 3016-3031,
612 10.1002/2013JD020710, 2014.
- 613 Campbell Scientific EC150 CO₂/H₂O Open-Path Gas Analyzer: <https://www.campbellsci.com/manuals>, access:
614 24.10.2018, 2018.
- 615 Chubb, T. H., Siems, S. T., and Manton, M. J.: On the Decline of Wintertime Precipitation in the Snowy
616 Mountains of Southeastern Australia, *J Hydrometeorol*, 12, 1483-1497, 10.1175/Jhm-D-10-05021.1, 2011.
- 617 Costin, A. B., and Gay, D.: *Studies in Catchment Hydrology in the Australian Alps, MPKV; Maharashtra*, 1961.
- 618 Cullen, N. J., and Conway, J. P.: A 22 month record of surface meteorology and energy balance from the ablation
619 zone of Brewster Glacier, New Zealand, *J Glaciol*, 61, 931-946, 2015.
- 620 Dee, D. P., Uppala, S. M., Simmons, A., Berrisford, P., Poli, P., Kobayashi, S., Andrae, U., Balmaseda, M.,
621 Balsamo, G., and Bauer, d. P.: The ERA-Interim reanalysis: Configuration and performance of the data
622 assimilation system, *Quarterly Journal of the royal meteorological society*, 137, 553-597, 2011.
- 623 Drobot, S. D., and Anderson, M. R.: Comparison of interannual snowmelt-onset dates with atmospheric
624 conditions, *Annals of Glaciology*, 33, 79-84, 2001.
- 625 Duus, A. L.: Estimation and analysis of snow cover in the Snowy Mountains between 1910 and 1991, *Aust
626 Meteorol Mag*, 40, 195-204, 1992.
- 627 Ellis, C. R., Pomeroy, J. W., Essery, R. L. H., and Link, T. E.: Effects of needleleaf forest cover on radiation and
628 snowmelt dynamics in the Canadian Rocky Mountains, *Can J Forest Res*, 41, 608-620, 10.1139/X10-227, 2011.
- 629 Falge, E., Baldocchi, D., Olson, R., Anthoni, P., Aubinet, M., Bernhofer, C., Burba, G., Ceulemans, G., Clement,
630 R., Dolman, H., Granier, A., Gross, P., Grunwald, T., Hollinger, D., Jensen, N. O., Katul, G., Keronen, P.,
631 Kowalski, A., Lai, C. T., Law, B. E., Meyers, T., Moncrieff, J., Moors, E., Munger, J. W., Pilegaard, K., Rannik,
632 U., Rebmann, C., Suyker, A., Tenhunen, J., Tu, K., Verma, S., Vesala, T., Wilson, K., and Wofsy, S.: Gap filling
633 strategies for long term energy flux data sets, *Agr Forest Meteorol*, 107, 71-77, Doi 10.1016/S0168-
634 1923(00)00235-5, 2001a.
- 635 Falge, E., Baldocchi, D., Olson, R., Anthoni, P., Aubinet, M., Bernhofer, C., Burba, G., Ceulemans, R., Clement,
636 R., Dolman, H., Granier, A., Gross, P., Grunwald, T., Hollinger, D., Jensen, N. O., Katul, G., Keronen, P.,
637 Kowalski, A., Lai, C. T., Law, B. E., Meyers, T., Moncrieff, H., Moors, E., Munger, J. W., Pilegaard, K., Rannik,
638 U., Rebmann, C., Suyker, A., Tenhunen, J., Tu, K., Verma, S., Vesala, T., Wilson, K., and Wofsy, S.: Gap filling
639 strategies for defensible annual sums of net ecosystem exchange, *Agr Forest Meteorol*, 107, 43-69, Doi
640 10.1016/S0168-1923(00)00225-2, 2001b.
- 641 Fayad, A., Gascoïn, S., Faour, G., López-Moreno, J. I., Drapeau, L., Le Page, M., and Escadafal, R.: Snow
642 hydrology in Mediterranean mountain regions: A review, *J Hydrol*, 551, 374-396, 2017.



- 643 Fiddes, S. L., Pezza, A. B., and Barras, V.: A new perspective on Australian snow, *Atmospheric Science Letters*,
644 16, 246-252, 10.1002/asl2.549, 2015.
- 645 Gellie, N. J. H.: Native vegetation of the Southern Forests: South-east highlands, Australian alps, south-west
646 slopes and SE corner bioregions, Royal Botanic Gardens, 2005.
- 647 Goree, P. A., and Younkin, R. J.: Synoptic Climatology of Heavy Snowfall Over the Central and Eastern United
648 States, 94, 663-668, 10.1175/1520-0493(1966)094<0663:Scosho>2.3.Co;2, 1966.
- 649 Granger, R. J., and Gray, D. M.: A Net-Radiation Model for Calculating Daily Snowmelt in Open Environments,
650 *Nord Hydrol*, 21, 217-234, 1990.
- 651 Gray, M. A., McGowan, H. A., Lowry, A. L., and Guyot, A.: Surface energy exchanges over contrasting
652 vegetation types on a sub-tropical sand island, *Agr Forest Meteorol*, 249, 81-99, 10.1016/j.agrformet.2017.11.018,
653 2018.
- 654 Grundstein, A. J., and Leathers, D. J.: A case study of the synoptic patterns influencing midwinter snowmelt
655 across the northern Great Plains, 12, 2293-2305, doi:10.1002/(SICI)1099-1085(199812)12:15<2293::AID-
656 HYP797>3.0.CO;2-9, 1998.
- 657 Hay, J. E., and Fitzharris, B. B.: The synoptic climatology of ablation on a New Zealand glacier, *Journal of*
658 *Climatology*, 8, 201-215, 10.1002/joc.3370080207, 1988.
- 659 Helgason, W., and Pomeroy, J.: Problems Closing the Energy Balance over a Homogeneous Snow Cover during
660 Midwinter, *J Hydrometeorol*, 13, 557-572, 10.1175/Jhm-D-11-0135.1, 2012.
- 661 Hendon, H. H., Thompson, D. W. J., and Wheeler, M. C.: Australian Rainfall and Surface Temperature Variations
662 Associated with the Southern Hemisphere Annular Mode, 20, 2452-2467, 10.1175/jcli4134.1, 2007.
- 663 Hennessy, K. J., Whetton, P. H., Walsh, K., Smith, I. N., Bathols, J. M., Hutchinson, M., and Sharples, J.: Climate
664 change effects on snow conditions in mainland Australia and adaptation at ski resorts through snowmaking, *Clim*
665 *Res*, 35, 255-270, 10.3354/cr00706, 2008.
- 666 Hope, P. K., Drosowsky, W., and Nicholls, N. J. C. D.: Shifts in the synoptic systems influencing southwest
667 Western Australia, 26, 751-764, 10.1007/s00382-006-0115-y, 2006.
- 668 Kidson, J. W.: An analysis of New Zealand synoptic types and their use in defining weather regimes, *International*
669 *journal of climatology*, 20, 299-316, 2000.
- 670 Liaw, A., and Wiener, M.: Classification and Regression by randomForest, *R News*, 2, 18-22, 2002.
- 671 Lopez-Moreno, J. I., and Vicente-Serrano, S. M.: Atmospheric circulation influence on the interannual variability
672 of snow pack in the Spanish Pyrenees during the second half of the 20th century, *Nord Hydrol*, 38, 33-44,
673 10.2166/nh.2007.030, 2007.



- 674 Male, D. H., and Granger, R. J.: Snow Surface-Energy Exchange, *Water Resour Res*, 17, 609-627, DOI
675 10.1029/WR017i003p00609, 1981.
- 676 Marks, D., and Dozier, J.: Climate and Energy Exchange at the Snow Surface in the Alpine Region of the Sierra-
677 Nevada .2. Snow Cover Energy-Balance, *Water Resour Res*, 28, 3043-3054, Doi 10.1029/92wr01483, 1992.
- 678 Mauder, M., and Foken, T.: Documentation and instruction manual of the eddy-covariance software package TK3,
679 2011.
- 680 Mazurkiewicz, A. B., Callery, D. G., and McDonnell, J. J.: Assessing the controls of the snow energy balance and
681 water available for runoff in a rain-on-snow environment, *J Hydrol*, 354, 1-14, 2008.
- 682 McGregor, G. R., and Gellatly, A. F.: The Energy Balance of a Melting Snowpack in the French Pyrenees During
683 Warm Anticyclonic Conditions, *International Journal of Climatology: A Journal of the Royal Meteorological*
684 *Society*, 16, 479-486, doi:10.1002/(SICI)1097-0088(199604)16:4<479::AID-JOC17>3.0.CO;2-W, 1996.
- 685 McKay, D. C., and Thurtell, G. W.: Measurements of the energy fluxes involved in the energy budget of a snow
686 cover, *J Appl Meteorol*, 17, 339-349, 1978.
- 687 Meneghini, B., Simmonds, I., and Smith, I. N.: Association between Australian rainfall and the Southern Annular
688 Mode, *International Journal of Climatology*, 27, 109-121, 10.1002/joc.1370, 2007.
- 689 Michelson, D. B.: Systematic correction of precipitation gauge observations using analyzed meteorological
690 variables, *J Hydrol*, 290, 161-177, 2004.
- 691 Moore, R., and Owens, I.: Controls on advective snowmelt in a maritime alpine basin, *Journal of Climate and*
692 *Applied Meteorology*
693 23, 135-142, 1984.
- 694 Neale, S. M., and Fitzharris, B. B.: Energy balance and synoptic climatology of a melting snowpack in the
695 Southern Alps, New Zealand, *International Journal of Climatology*, 17, 1595-1609, 10.1002/(SICI)1097-
696 0088(19971130)17:14<1595::AID-JOC213>3.0.CO;2-7, 1997.
- 697 Nicholls, N.: Climate variability, climate change and the Australian snow season, *Aust Meteorol Mag*, 54, 177-
698 185, 2005.
- 699 Pachauri, R. K., Allen, M. R., Barros, V. R., Broome, J., Cramer, W., Christ, R., Church, J. A., Clarke, L., Dahe,
700 Q., and Dasgupta, P.: Climate change 2014: synthesis report. Contribution of Working Groups I, II and III to the
701 fifth assessment report of the Intergovernmental Panel on Climate Change, IPCC, 2014.
- 702 Parry, M., Parry, M. L., Canziani, O., Palutikof, J., Van der Linden, P., and Hanson, C.: Climate change 2007-
703 impacts, adaptation and vulnerability: Working group II contribution to the fourth assessment report of the IPCC,
704 Cambridge University Press, 2007.



- 705 Pook, M. J., McIntosh, P. C., and Meyers, G. A.: The synoptic decomposition of cool-season rainfall in the
706 southeastern Australian cropping region, *Journal of Applied Meteorology Climatology*, 45, 1156-1170, 2006.
- 707 Pook, M. J., Risbey, J., and McIntosh, P.: East coast lows, atmospheric blocking and rainfall: a Tasmanian
708 perspective, *IOP Conference Series: Earth and Environmental Science*, 2010, 012011,
- 709 Pook, M. J., Risbey, J. S., and McIntosh, P. C.: The synoptic climatology of cool-season rainfall in the central
710 wheatbelt of Western Australia, *Monthly Weather Review*, 140, 28-43, 2012.
- 711 Pook, M. J., Risbey, J. S., and McIntosh, P. C.: A comparative synoptic climatology of cool-season rainfall in
712 major grain-growing regions of southern Australia, *Theoretical Applied Climatology*, 117, 521-533,
713 10.1007/s00704-013-1021-y, 2014.
- 714 Prezerakos, N. G., and Angouridakis, V. E.: Synoptic consideration of snowfall in Athens, *Journal of Climatology*,
715 4, 269-285, 10.1002/joc.3370040305, 1984.
- 716 Rasmussen, R., Baker, B., Kochendorfer, J., Meyers, T., Landolt, S., Fischer, A. P., Black, J., Theriault, J. M.,
717 Kucera, P., Gochis, D., Smith, C., Nitu, R., Hall, M., Ikeda, K., and Gutmann, E.: How Well Are We Measuring
718 Snow? The NOAA/FAA/NCAR Winter Precipitation Test Bed, *B Am Meteorol Soc*, 93, 811-829, 10.1175/Bams-
719 D-11-00052.1, 2012.
- 720 Reba, M. L., Link, T. E., Marks, D., and Pomeroy, J.: An assessment of corrections for eddy covariance measured
721 turbulent fluxes over snow in mountain environments, *Water Resour Res*, 45, Artn W00d38
722 10.1029/2008wr007045, 2009.
- 723 Reinfelds, I., Swanson, E., Cohen, T., Larsen, J., and Nolan, A.: Hydrosatial assessment of streamflow yields
724 and effects of climate change: Snowy Mountains, Australia, *J Hydrol*, 512, 206-220,
725 10.1016/j.jhydrol.2014.02.038, 2014.
- 726 Robock, A.: The seasonal cycle of snow cover, sea ice and surface albedo, *Monthly Weather Review*, 108, 267-
727 285, 1980.
- 728 Romolo, L., Prowse, T. D., Blair, D., Bonsal, B. R., Marsh, P., and Martz, L. W.: The synoptic climate controls
729 on hydrology in the upper reaches of the Peace River Basin. Part II: Snow ablation, 20, 4113-4129,
730 doi:10.1002/hyp.6422, 2006a.
- 731 Romolo, L., Prowse, T. D., Blair, D., Bonsal, B. R., and Martz, L. W.: The synoptic climate controls on hydrology
732 in the upper reaches of the Peace River Basin. Part I: snow accumulation, 20, 4097-4111, doi:10.1002/hyp.6421,
733 2006b.
- 734 Ruckstuhl, C., Philipona, R., Morland, J., and Ohmura, A.: Observed relationship between surface specific
735 humidity, integrated water vapor, and longwave downward radiation at different altitudes, *Journal of Geophysical
736 Research: Atmospheres*, 112, 2007.



- 737 Sade, R., Rimmer, A., Litaor, M. I., Shamir, E., and Furman, A.: Snow surface energy and mass balance in a warm
738 temperate climate mountain, *J Hydrol*, 519, 848-862, 2014.
- 739 Snowy Hydro Limited Snow Depths Calculator: [https://www.snowyhydro.com.au/our-](https://www.snowyhydro.com.au/our-energy/water/inflows/snow-depths-calculator/)
740 [energy/water/inflows/snow-depths-calculator/](https://www.snowyhydro.com.au/our-energy/water/inflows/snow-depths-calculator/), access: 03/08/2018, 2018.
- 741 Stewart, I. T.: Changes in snowpack and snowmelt runoff for key mountain regions, *Hydrol Process*, 23, 78-94,
742 10.1002/hyp.7128, 2009.
- 743 Stiperski, I., and Rotach, M. W.: On the Measurement of Turbulence Over Complex Mountainous Terrain, *Bound-*
744 *Lay Meteorol*, 159, 97-121, 10.1007/s10546-015-0103-z, 2016.
- 745 Stoy, P. C., Peitzsch, E., Wood, D., Rottinghaus, D., Wohlfahrt, G., Goulden, M., and Ward, H.: On the exchange
746 of sensible and latent heat between the atmosphere and melting snow, *Agricultural Forest Meteorology*, 252, 167-
747 174, 2018.
- 748 Stull, R.: Wet-Bulb Temperature from Relative Humidity and Air Temperature, *J Appl Meteorol Clim*, 50, 2267-
749 2269, 10.1175/Jamc-D-11-0143.1, 2011.
- 750 Sturm, M., Holmgren, J., and Liston, G. E.: A seasonal snow cover classification system for local to global
751 applications, *J Climate*, 8, 1261-1283, 1995.
- 752 Theobald, A., McGowan, H., Speirs, J., and Callow, N.: A Synoptic Classification of Inflow-Generating
753 Precipitation in the Snowy Mountains, Australia, *J Appl Meteorol Clim*, 54, 1713-1732, 10.1175/Jamc-D-14-
754 0278.1, 2015.
- 755 Theobald, A., McGowan, H., and Speirs, J.: Trends in synoptic circulation and precipitation in the Snowy
756 Mountains region, Australia, in the period 1958-2012, *Atmos Res*, 169, 434-448, 10.1016/j.atmosres.2015.05.007,
757 2016.
- 758 Ueno, K.: Synoptic conditions causing nonmonsoon snowfalls in the Tibetan Plateau, *Geophys Res Lett*, 32, 2005.
- 759 Viviroli, D., Durr, H. H., Messerli, B., Meybeck, M., and Weingartner, R.: Mountains of the world, water towers
760 for humanity: Typology, mapping, and global significance, *Water Resour Res*, 43, Artn W07447
761 10.1029/2006wr005653, 2007.
- 762 Webb, E. K., Pearman, G. I., and Leuning, R.: Correction of flux measurements for density effects due to heat
763 and water vapour transfer, *Quarterly Journal of the Royal Meteorological Society*, 106, 85-100, 1980.
- 764 Webb, M., Slingol, A., and Stephens, G.: Seasonal variations of the clear-sky greenhouse effect: The role of
765 changes in atmospheric temperatures and humidities, *Climate dynamics*, 9, 117-129, 1993.



766 Welch, C. M., Stoy, P. C., Rains, F. A., Johnson, A. V., and McGlynn, B. L.: The impacts of mountain pine beetle
767 disturbance on the energy balance of snow during the melt period, *Hydrol Process*, 30, 588-602,
768 10.1002/hyp.10638, 2016.

769 Whetton, P. H., Haylock, M. R., and Galloway, R.: Climate change and snow-cover duration in the Australian
770 Alps, *Climatic Change*, 32, 447-479, Doi 10.1007/Bf00140356, 1996.

771 Wilks, D. S.: Cluster analysis, in: *International geophysics*, Elsevier, 603-616, 2011.

772 Worboys, G. L., and Good, R. B.: *Caring For Our Australian Alps Catchments: Summary Report For Policy*
773 *Makers*, 2011.

774

775

776

777

778

779

780

781

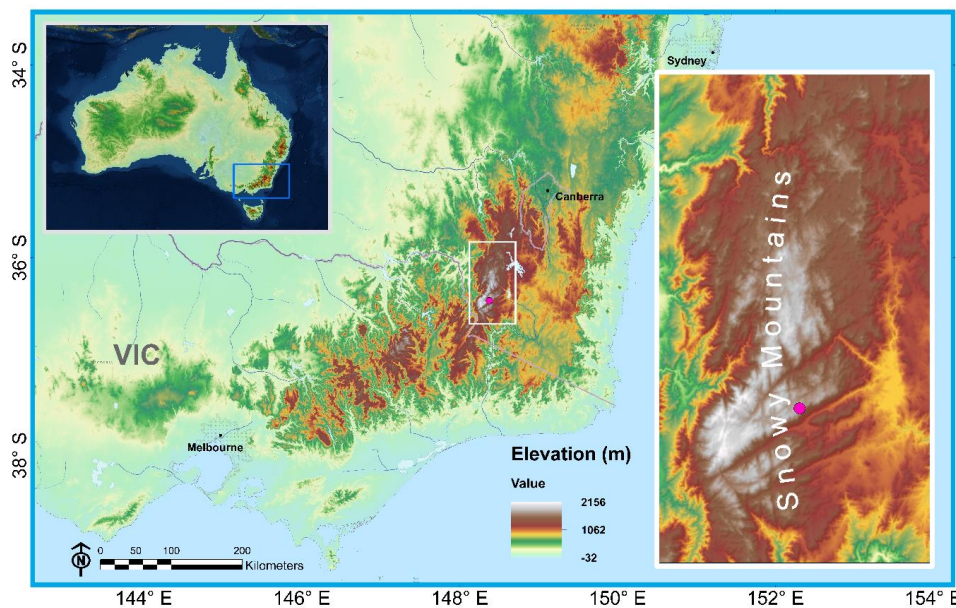
782

783

784



785
786
787
788
789
790
791
792

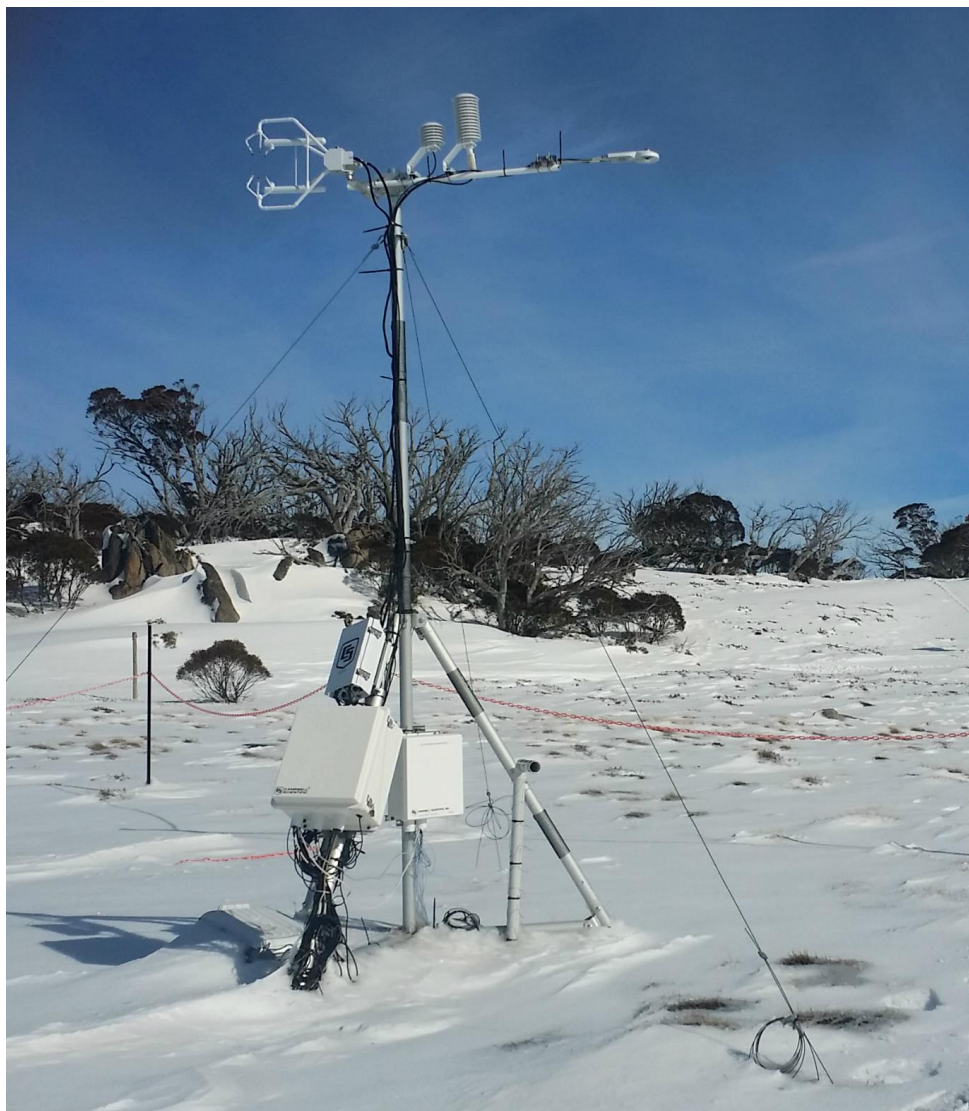


793 **Figure 1: Map of southeast Australia and the Snowy Mountains. Pink dot represents the location of the energy balance**
794 **instrumentation site. Map layer sources copyright: ESRI, USGS, NOAA, DigitalGlobe, GeoEye, Earthstar**
795 **Geographics, CNE S/A Airbus DS, USDA, AeroGRID, IGN, and the GIS User Community.**

796
797
798
799
800



801
802
803
804

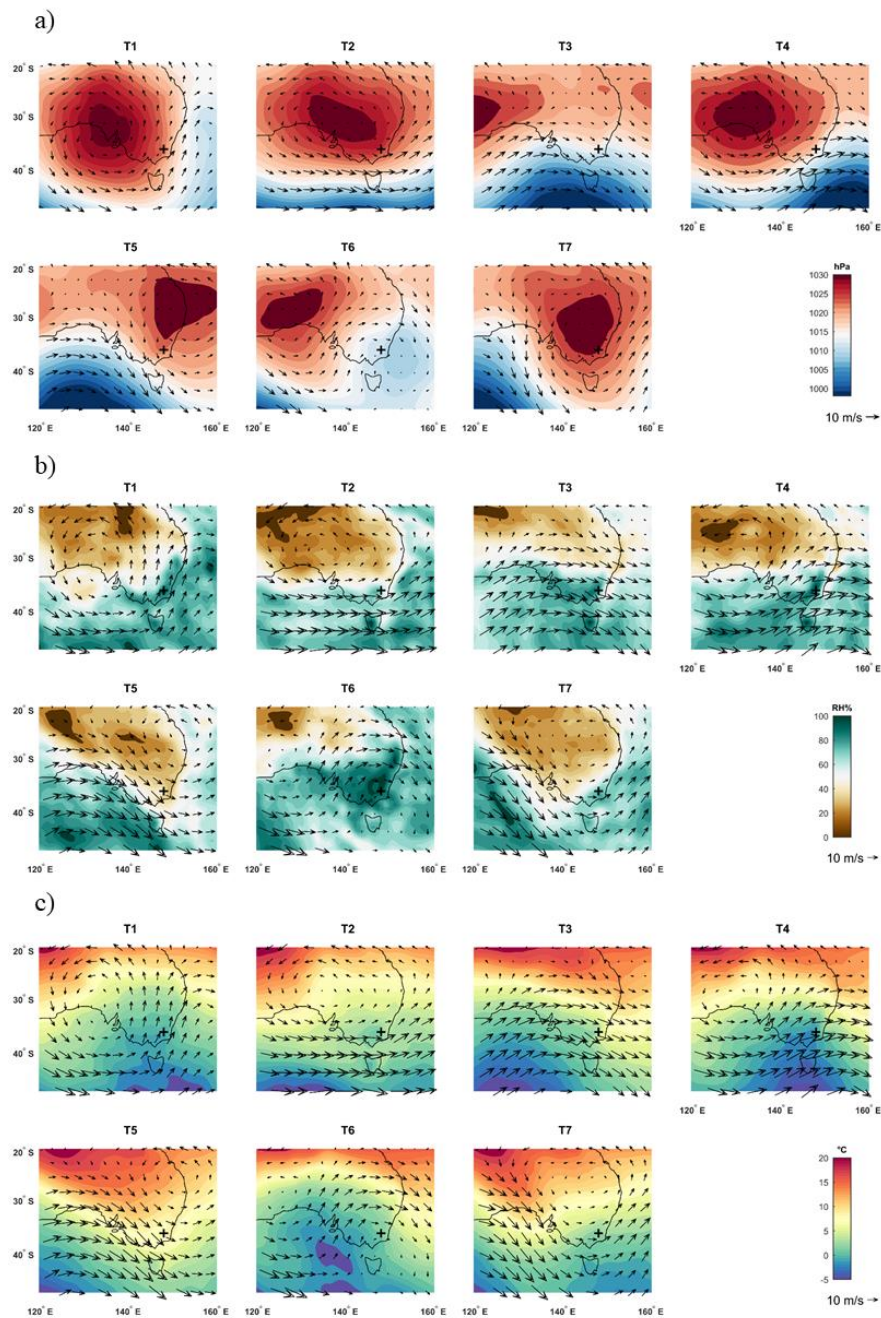


805
806
807

Figure 2: Energy balance field site with eddy covariance instrumentation at Pipers Creek catchment headwaters.



808



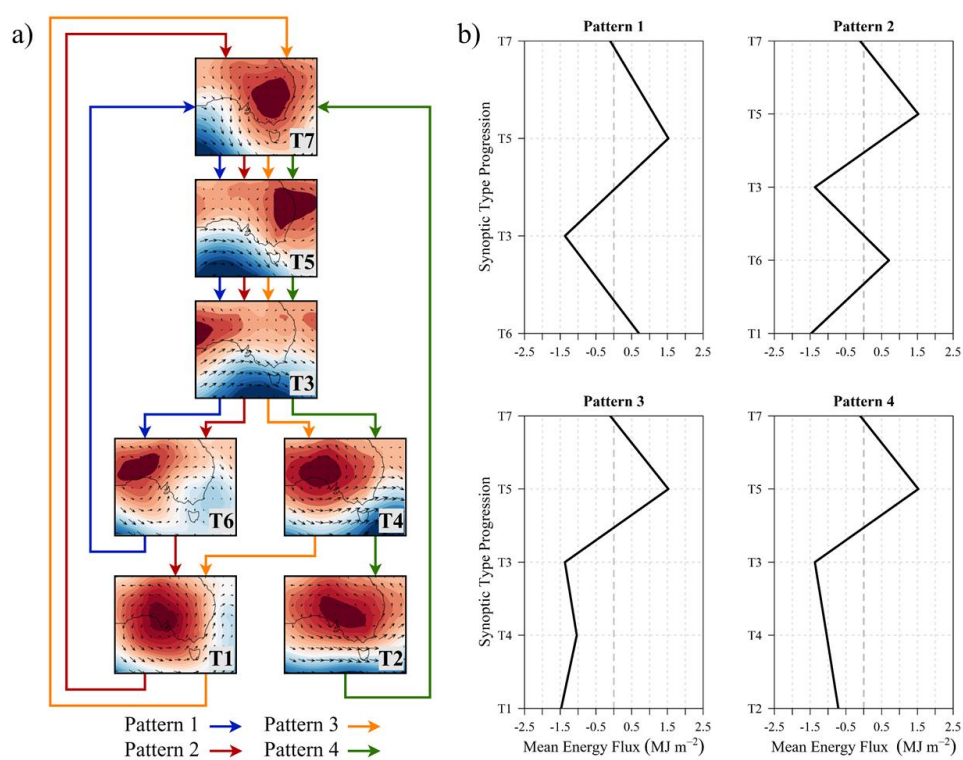
809



810 **Figure 3: Mean synoptic type MSLP and 10m wind vectors (a), 850 hPa RH and wind vectors (b), and 850 hPa T_d and**
811 **wind vectors (c) over the southeast Australia region for the 2016 and 2017 seasons. Location of surface energy balance**
812 **site marked with ‘+’.**



813



814

815 **Figure 4: Flowchart of four primary synoptic type patterns/progressions based on probability of transition for the 2016**
816 **and 2017 seasons (a) and calculated synoptic pattern snowpack fluxes based on median daily values and mean duration**
817 **of synoptic type (b).**

818

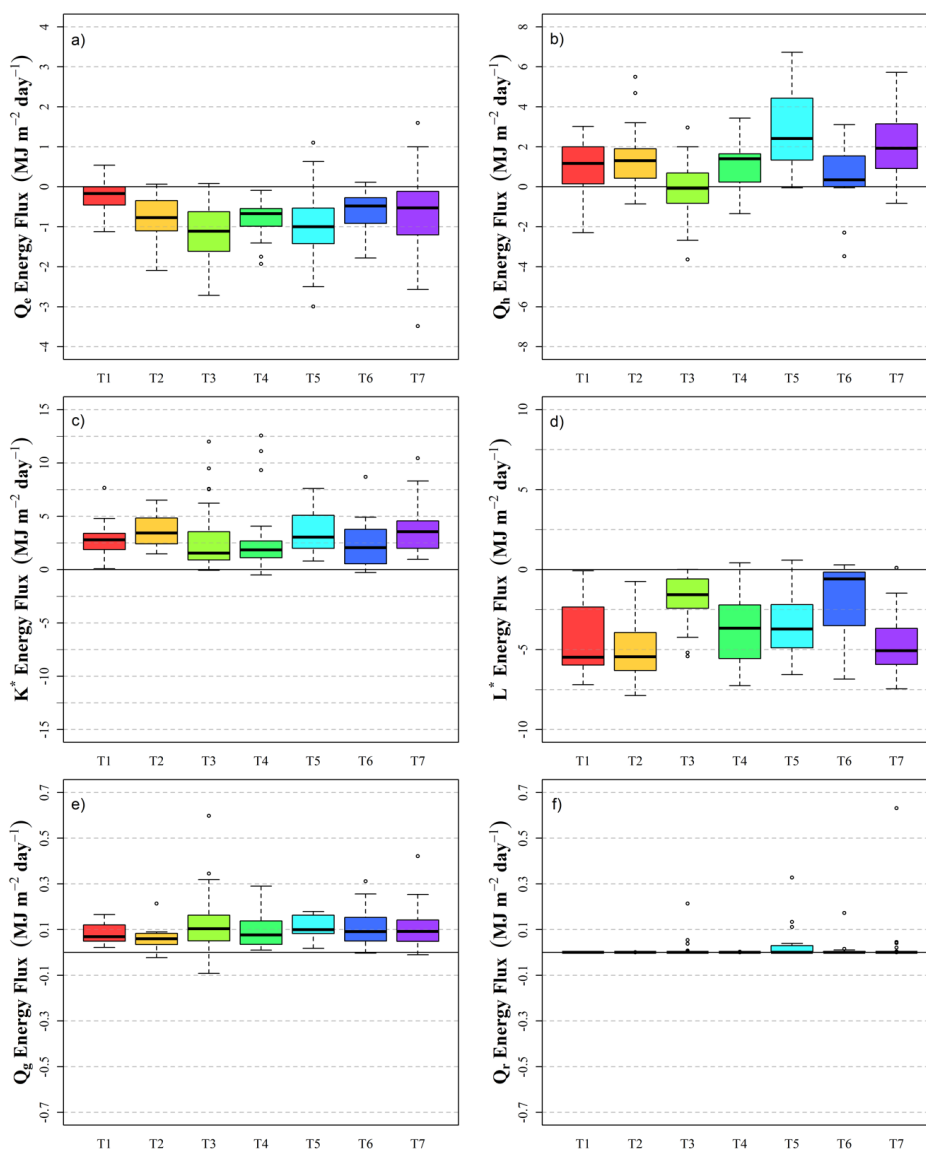
819



820

821

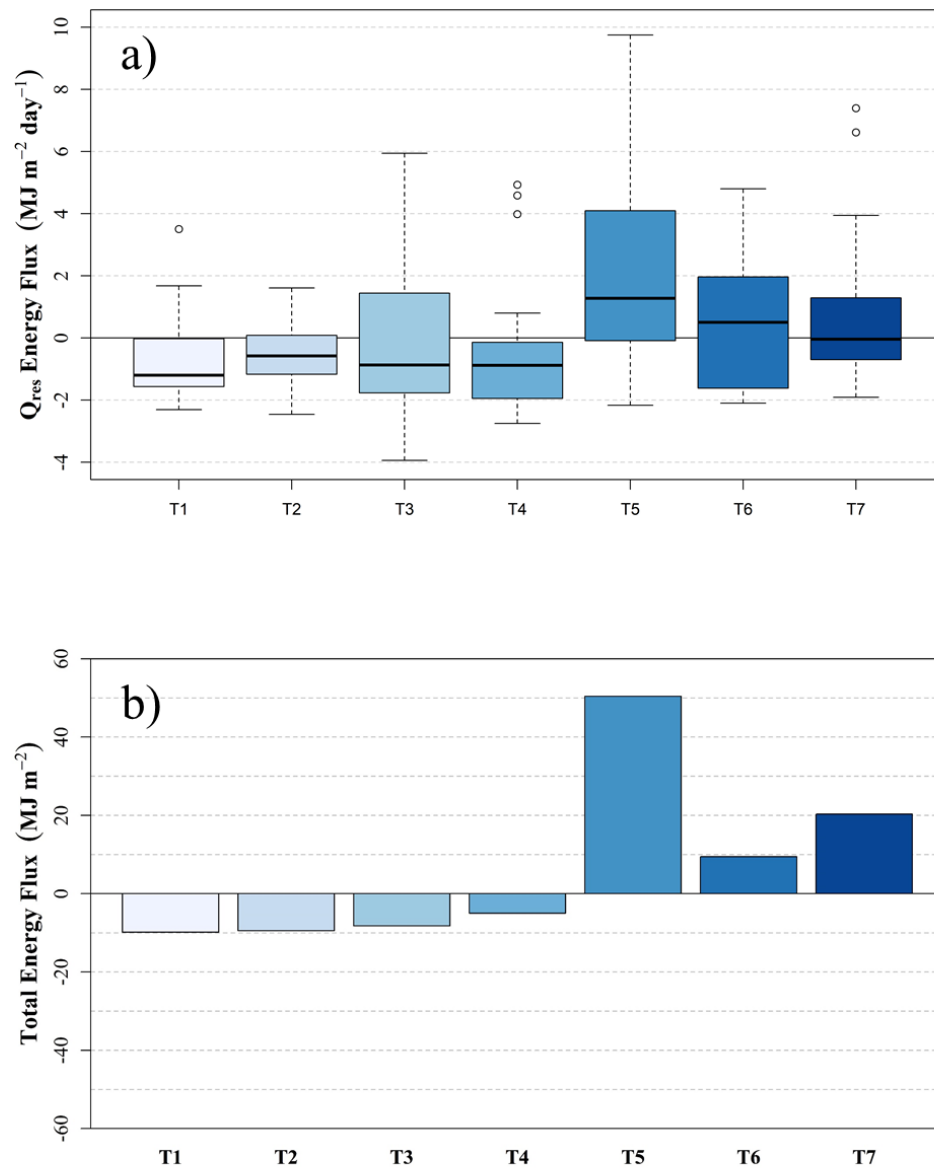
822



823 **Figure 5: Daily snowpack energy fluxes by term for each synoptic type for the 2016 and 2017 seasons.**

824

825



826

827 **Figure 6: Daily snowpack energy fluxes (a) and total energy flux (b) by synoptic type for the 2016 and 2017 seasons.**

828

829



830

Instrument	Manufacturer	Variables Measured	Accuracy
SI-111	Apogee Instruments	Surface Temperature (T_{sfc})	$\pm 0.2^{\circ}\text{C}$ $-10^{\circ}\text{C} < T < 65^{\circ}\text{C}$ $\pm 0.5^{\circ}\text{C}$ $-40^{\circ}\text{C} < T < 70^{\circ}\text{C}$
CS650	Campbell Scientific	Soil Water Content (SWC)	$\pm 3\%$ SWC
		Soil Temperature	$\pm 5^{\circ}\text{C}$
CSAT3A	Campbell Scientific	Wind Components (u_x , u_y , u_z); Wind Speed (u) and Direction ($^{\circ}$); and Sonic Temperature	$\pm 5 \text{ cm s}^{-1}$
EC150	Campbell Scientific	H ₂ O Gas Density	2%
NOAH II	ETI Instrument Systems	Precipitation Accumulation	$\pm 0.254 \text{ mm}$
HFP01	Hukseflux	Soil Heat Flux	$< 3\%$
CNR4	Kipp and Zonen	K_{\downarrow} , K_{\uparrow} , L_{\downarrow} , L_{\uparrow}	$K < 5\%$ Daily Total $L < 10\%$ Daily Total
HMP155	Vaisala	Air Temperature (T_d)	$< 0.3^{\circ}\text{C}$
		Relative Humidity (RH)	$< 1.8\%$ RH
PTB110	Vaisala	Barometric Pressure	$\pm 0.15 \text{ kPa}$

831

832 **Table 1: Information on instruments used at the Pipers Creek catchment site.**

833

834

835

836

837

838

839

840

841

842

843

844

845



846

Synoptic Type	T1	T2	T3	T4	T5	T6	T7
Surface Characteristics	High pressure; SW winds	High pressure; WNW winds	Frontal; NW winds	High/low transition; W winds	High Pressure; NNW winds	Lee-side low; SW winds	High pressure; WNW winds
Cloud Cover (% days with any cover)	87.50%	76.47%	89.13%	100.00%	87.50%	100.00%	76.47%
Q_h (MJ m ⁻² day ⁻¹)	1.17	1.30	0.04	0.88	2.50	0.47	1.92
Q_e (MJ m ⁻² day ⁻¹)	-0.22	-0.64	-1.16	-0.67	-1.09	-0.51	-0.53
K_{\downarrow} (MJ m ⁻² day ⁻¹)	12.62	15.47	8.91	11.29	12.60	8.11	13.05
K_{\uparrow} (MJ m ⁻² day ⁻¹)	-9.61	-11.26	-6.97	-9.55	-9.48	-5.85	-9.60
L_{\downarrow} (MJ m ⁻² day ⁻¹)	19.53	20.16	24.95	22.08	23.59	26.57	21.38
L_{\uparrow} (MJ m ⁻² day ⁻¹)	-25.32	-26.00	-26.63	-25.74	-27.38	-26.91	-26.70
Q_g (MJ m ⁻² day ⁻¹)	0.07	0.06	0.10	0.08	0.10	0.09	0.09
Q_r (MJ m ⁻² day ⁻¹)	0.00	0.00	0.00	0.00	0.01	0.00	0.00
Q_m (MJ m ⁻² day ⁻¹)	-1.31	-0.43	-0.84	-0.90	1.11	0.63	-0.20
Total Number of Occurrences	15	16	44	19	22	16	31
Mean Type Duration (Days)	1.23	1.31	1.59	1.19	1.20	1.33	1.42

847

848 **Table 2: Synoptic, energy flux, and occurrence characteristics for each synoptic type. Mean Daily surface and cloud**
 849 **cover characteristics are mean values and daily energy flux values are median values.**